Int J Adv Manuf Technol (2016) 86:1963–1972
DOI 10.1007/s00170-015-8323-4

ORIGINAL ARTICLE

Investigating surface metrology of curved wall surface during milling of SS304 with different tool path strategies

Zachary Brooks[1] · **Chandra Nath**[1,2] · **Thomas R. Kurfess**[1]

Received: 2 June 2015 / Accepted: 29 December 2015 / Published online: 12 January 2016

Abstract Curved mating surfaces that exist in complex engine parts such as turbine blades play a critical role in part fitting and assembly and, thus, system performance. Control of precise surface metrology (e.g., form error, surface roughness) during machining of such surfaces is highly challenging, especially when processing super alloys like hardened steels. This work aims to experimentally investigate surface metrology of a 12.70-mm-thick curved plate platform (with S-shaped sidewall) of AISI SS304 material during milling on a vertical three-axis milling machine with three different tool path strategies: ramp, contour, and peripheral. Experiments are performed to study surface location error (SLE) and roughness during upward and downward feeding of tool on both concave and convex sidewall surfaces at different spindle speed and feed combinations. SLE values that are estimated as undercut or overcut with respect to the desired surface are found to be minimum with ramp (15.05 μm), followed by contour (18.63 μm), and maximum with peripheral (24.12 μm) milling paths. However, peripheral milling may be preferable in terms of surface roughness (improved about 40 %) and overall machining time (six times faster than ramp milling). The findings are analyzed based on the associated cutting mechanics and cutting forces.

Keywords Curved surface · Surface error · Alloy steels · Milling tool path

✉ Thomas R. Kurfess
kurfess@gatech.edu

[1] George W. Woodruff School of Mechanical Engineering, Georgia Institute of Technology, Atlanta, GA 30309, USA

[2] Present address: Hitachi America Ltd. Research and Development Division, Farmington Hills, MI 48335, USA

1 Introduction

Side wall surfaces—both straight and curved—are common in many complex engines as mating surfaces between adjacent parts. For example, in turbo-machineries, all turbine blades contain a platform base that has mating wall surfaces in two sides allowing two more blades to be assembled [1]. These mating surfaces are required to create airtight seals to prevent gas/fluid leaks into the raceway of the turbine disk. Deviations from target geometry can result in system noises, energy loss, and poor performance at best and, at worst, catastrophic failure that may lead to system damage, bodily injury, or even death [2]. Therefore, mating surfaces, especially curved ones, play a critical role in part fitting and assembly. Furthermore, surface roughness is highly related to the system assembly, performance, and the part life. However, rectifying these inaccuracies (i.e., surface location error or form error, surface roughness) to achieve a high level of dimensional accuracy and productivity of these complex components is highly challenging, especially when processing alloy steels like stainless steels. When machining these alloys, high chip load, high strength and hardness, higher degree of ductility, work hardenability, and low thermal conductivity cause issues such as higher cutting forces, machining chatter, thermal cracks, and build-up edge [3–8]. As a result, the final machined part can have unexpected dimensional error (e.g., surface location error) and poor surface finish [3–7].

Much research has been conducted on milling to produce sculptured and curved surfaces from different materials using different tool path strategies: ramp, contour, and peripheral [4–24]. Kita et al. [4] studied cutting force and tool wear relationship during ball end milling of SKD 61 hardened steel. Ikua et al. [5, 6] studied the machining error with ramp and contour milling paths on a half-cylindrical workpiece of JIS S45C carbon steel and epoxy material. Lim and Menq [7]

have also studied ramp and contour paths on AISI 1018 carbon steel. Experimental studies were also performed on aluminum alloys [8, 9] and titanium alloys [10, 11]. Several cutting force models, chip geometry models, and surface finish models are also presented for machining with ball nose end mills on curved sculpted surfaces in [12–17].

Many studies also consider a peripheral milling path to eliminate or control the dimensional error by adopting online adaptive control of machining parameters based on tool deflection monitoring, cutting forces, and offline tool path compensation [18–24]. Online adaptive control requires the addition of sensors and hardware and software changes on the machine; therefore, it is not always viable due to financial and physical limitations. Abou-El-Hossein focused on high-speed end milling of SS 304 for investigating with the changes in tool geometry. Previous studies suggest that there is a very few research that focuses on finding the best milling tool path strategies during milling of a curved surface that features both concave and convex surfaces. Moreover, research is so far limited in processing important stainless steels like SS304.

The aim of this work is to experimentally investigate surface metrology of an S-curved surface (representing a turbine blade platform) of SS304 material during milling on a vertical three-axis milling machine with three different tool path strategies: ramp, contour, and peripheral. Experiments are performed to study dimensional accuracy including surface location error (SLE) and roughness during upward and downward feeding of tool on both concave and convex sidewall surfaces at different spindle speed and feed combinations. SLE values are estimated as undercut or overcut with respect to the desired surface. Surface roughness and overall machining time are also measured in order to optimize the best milling tool path strategy. Based on the dynamic stability provided by stability lobe diagrams and cutting forces, the performance is analyzed.

The remainder of the paper is organized as follows. Section 2 describes the experimental setup and procedure for milling experiments related to ramp, contour, and peripheral milling strategies; cutting conditions; and data collection systems. In Sect, 3, findings from milling experiments are presented, analyzed, and compared, followed by a comprehensive conclusion and future research scope in final Sect. 4.

2 Experimental setup and procedure

Milling experiments are performed on a three-axis CNC vertical milling machine, *Okuma Millac 44V*. Three different milling path techniques including ramp, contour, and peripheral milling are tested on an S-curved work surface that features both concave and convex surfaces and requires machining with upward and downward feeding of tool, as seen in Fig. 1a. The workpiece is made of stainless steel 304 and measures 152.40 mm in length and 12.70 mm thick. Ball nose end mills (*Accupro 03288263*) extending 45.72 mm out of the tool holder are used for ramp and contour milling (Fig. 2). However, square end mills (*Kennametal AADE0500J3DRB*) extending 88.90 mm out of the tool holder are used for peripheral milling experiments, because the ball nose mills are usually too short to apply in the present experimental setup (Fig. 3). For all tests, zirconium nitride (ZrN)-coated carbide tools with geometry: 12.70-mm diameter, three flutes, and a 37° helix angle were used.

By varying cutting speed and feed per tooth, a 2^2 full factorial design of experiment (DoE) was considered for all three milling strategies. For the peripheral cutting tests, the DOE was designed for two different radial depths of cut (i.e., eight tests) as listed in Table 1. Cutting parameters are selected based on previous studies in milling [3, 24]. It can be noted that the low- and high-level values of cutting speed are kept constant regardless of the milling type. Due to this, spindle speeds for ramp and contour milling are different from peripheral milling. In case of peripheral milling, the formula is as follows: cutting speed = $\pi \times$ tool dia $\times$ spindle speed. On the other hand, for ramp and contour milling, the cutting speed becomes smaller at the spindle speeds used for peripheral milling due to the smaller tool-workpiece contact zone at 0.508-mm axial depth of cut (DOC). Also, the cutting speed varies due to the cutting locations. In this study, cutting speed is estimated based on the tool engagement with a flat workpiece (e.g., bottom or topmost point of the S-curved plate). For an axial DOC of 0.508 mm, the diameter of the tool that gets engaged at surface location is estimated to be about 5 mm. Stability lobe diagrams (SLD) [25] obtained by impulse excitation (hammer tests) on both the tool and workpiece are also examined to make sure that the tests are performed in stable region of milling parameters (see Fig. 2). All experiments are repeated about two to three times for confirming the findings. For cooling and lubrication at the tool-workpiece-chip interfaces during machining, a synthetic cutting fluid (Castrol Syntilo 9954) at 5 % by volume concentration with water was used.

Profiles of the machined surfaces were obtained using *Brown and Sharpe* coordinate measurement machine (CMM) probe. Surface roughness values were obtained using *Form Talysurf* surface profilometer. Force data are collected by arranging the following components: (i) a *Kistler* three-component force dynamometer (type 9257B), (ii) a data cable, (iii) a *Kistler* three-component charge amplifier, (iv) a National Instruments (NI) compact data acquisition (cDAQ) module, and (v) a *LabView* software on the computer. The type of milling used was down-milling, where the cutting forces on each tooth decrease with tool rotation. This approach is recommended for the difficult-to-machine materials that are prone to produce vibrations of the tool and that in turn causes variations in chip thickness and surface finish [26].

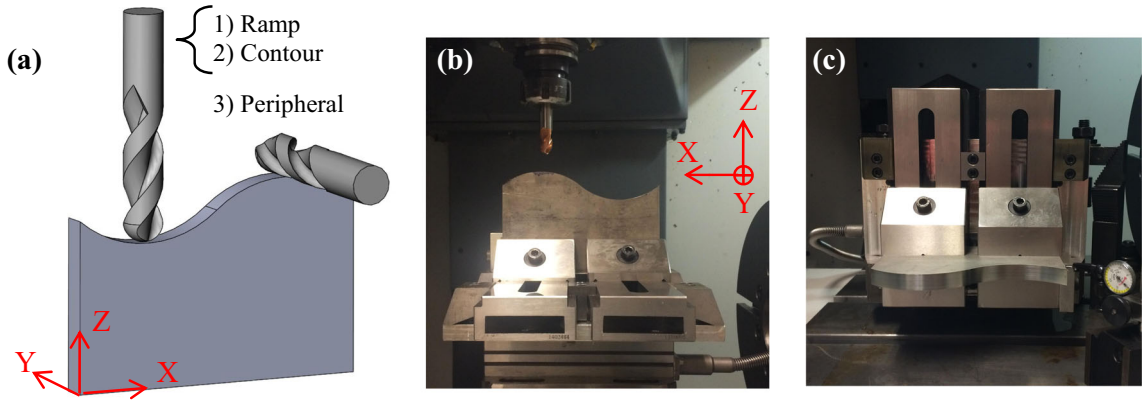

Fig. 1 **a** Milling tool path strategies, **b** ramp and contour path fixturing, and **c** peripheral path fixturing

3 Results and discussions

In this section, surface location error (SLE) and surface roughness of the machined surfaces obtained with ramp, contour, and peripheral milling techniques are presented. To quantify the SLE, CMM profiles are obtained before and after the machining of the S-curved surface. These CMM data are then interpolated at thousands of *x*-axis locations at which the SLE value is obtained by calculating the vertical (*z*-axis) difference between the theoretical (or expected) value and the measured value on the actual milled surface. Note that a positive SLE value indicates undercutting of the material while a negative value is for overcutting. The measured cutting force components are also analyzed to explain the machining responses. For convenience of analysis, as seen in Fig. 3, the S-curved surface (152.4 mm) is divided into four equal regions: (i) concave downward, (ii) concave upward, (iii) convex upward, and (iv) convex downward.

3.1 Ramp milling

Figure 4 depicts the SLE plots along the surface for the four different cutting conditions in ramp milling. SLE values at five selected locations on the *x*-axis are presented in Table 2. Note that the CMM probe is allowed some initial region over the machined surface to start obtaining reliable data; thus, the data profiles are not seen at $X=0$ mm. The first available data for all 16 tests is found to be at a distance of 12.75 mm. As seen in Fig. 4, a general trend of undercutting the material is observed when the tool ramps down (i.e., regions I and IV) off both the concave and convex surfaces. In contrast, overcutting occurs during the ramp up (regions II and III) for all tests. This reveals that the material removal mechanics in the tested S-curved surface depends on the ramping direction of the tool.

The major factor that contributes to the cutting mechanics during ramping down is skidding of the tool on the surface. Much like drilling, a ball end mill has a high tendency to skid (or slide) due to its "ball shape" geometry when cutting an inclined surface toward downward direction. Also, the skidding phenomenon with ball geometry can be influenced by the following: (i) contact location on the ball surface with respect to the tool center axis (i.e., force direction and amount change with the location) and (ii) contact interface area between the tool and the workpiece at a specific location. The skidding would increase with the increase in the inclination angle (θ in Fig. 3) between the normal vector of the curved surface and the tool rotational axis. When skidding takes place while ramping down an incline, the tool cannot shear the material at the intended DOC due to the fact that the tool edge cannot effectively engage into the workpiece. Rather, the tool is

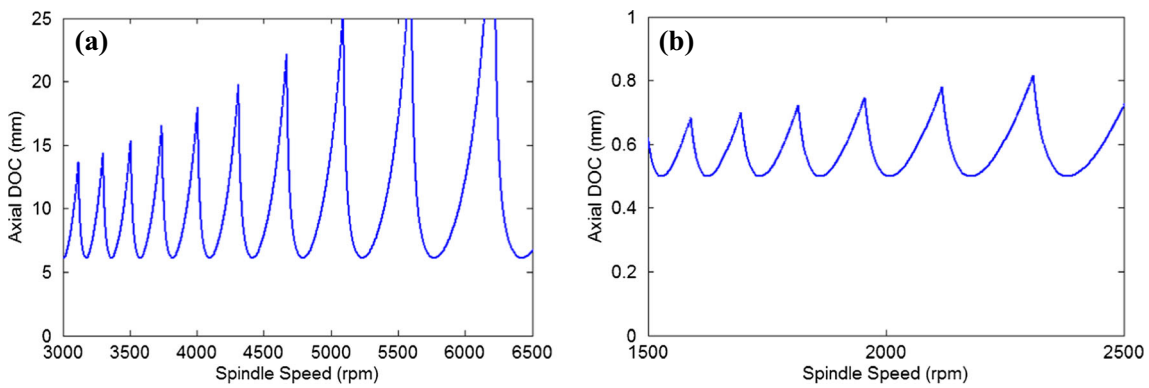

Fig. 2 Stability lobe diagrams obtained for **a** ramp and contour milling tests (with ball end mill) and **b** peripheral milling tests (with square-end mill)

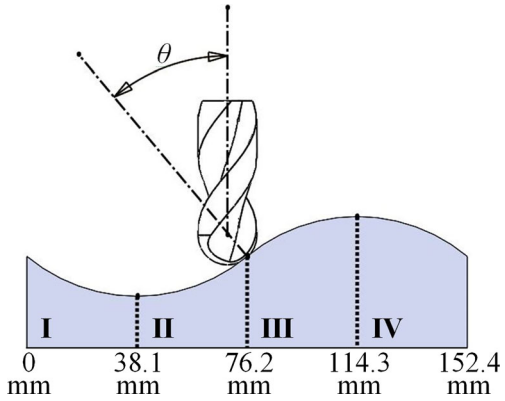

Fig. 3 The S-curved surface with four workpiece regions and inclination angle

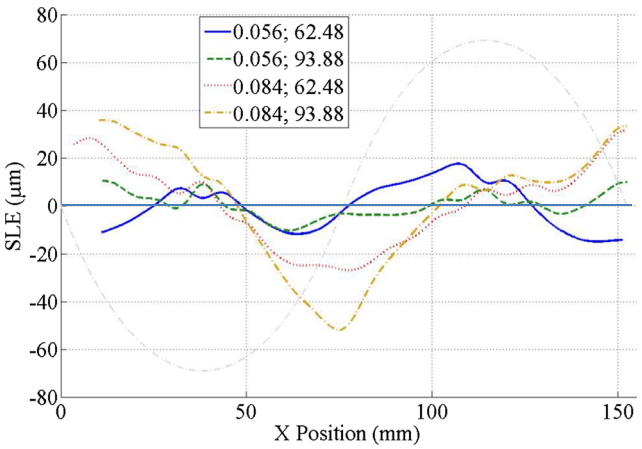

Fig. 4 Surface location error for ramp milling path

pushed by the material away (in *x*-axis) from the surface location while cutting. The skidding action also causes the tool to bend at the end depending on the tool and workpiece material strength. Tool bending analysis studied by Ikua et al. [2] during ball end milling of an inclined surface can support such skidding phenomenon discussed above. This results in undercut of the material.

On the other hand, when the ball end mill ramps up an inclined surface, the tool is dragged or pulled into the workpiece by its *x*-axis motion. This causes the material on the surface of the workpiece to compress slightly, resulting in what appears as overcutting the material. The SLE values in all four regions follow that the probability of such overcut error decreases with decreasing the inclination angle.

Additionally, the chip load differs depending on the ramping direction, as seen in Fig. 5a, b for ramping down and up, respectively. When ramping down (regions I and IV), the tool cutting edge engages with the workpiece more in the lower region than the theoretical contact region or point (refer Fig. 3). In such situation, chip area becomes larger. In contrast, in the case of ramping up (regions II and III), the tool engages with the workpiece mainly in the upper region. As the tool edge is more straight or linear in that region, the chip area becomes smaller. Due to the larger chip area when ramping down, higher forces result when compared to ramping up. The experimental force data seen (for about 0–25 vs. 50–100 mm) in Fig. 6 agree with this phenomenon. With the assumption that the tool acts as a cantilever beam, a higher force caused more tool deflection away from the workpiece causing in an undercut error. Toh [27] also concluded this phenomenon in his research.

The two prominent peaks in the force plots are at the bottom of the concave curve ($x = 38.1$ mm) and the top of the convex curve ($x = 114.3$ mm). At these locations, the inclination angle is zero resulting in tip of the tool engaging the material. At the tip of a ball nose, the speed is zero, which results in ploughing material away instead of completely shearing it. Furthermore, out of the three flutes in the ball nose mills used in the experiments, only one flute consists of extended cutting edge until the tool center or tip point, while others do not extend to the tip for chip evacuation purposes (see Fig. 7). The start of the sharp peaks is at an angle where the other flutes are no longer engaging and the end of the peaks is where all three cutting edges are engaged again. This tool tip geometry in ball nose end mill significantly affects the tool tip with higher compressive stress, resulting in higher forces.

When comparing the SLE values against ramp milling parameters, it is observed that, at any given cutting speed, the increase in feed rate from 0.056 to 0.084 mm/tooth (i.e., 1.5 times) significantly increases the SLE values at all five

Table 1 Machining conditions for ramp, contour, and peripheral milling experiments

Milling type	Spindle speed (rpm)	Cutting speed (m/min)	Cutting speed (m/min)	Feed speed (mm/min)	Feed speed (mm/min)	Radial depth (mm)
1. Ramp	3995	62.48	0.056	669.72	0.508	0.254
2. Contour (each four tests)	6000	93.88	0.056	1016		
	3995	62.48	0.084	1004.62		
	6000	93.88	0.084	1509.27		
3. Peripheral (total eight tests)	1566	62.48	0.056	262.53	12.70 (blade thickness)	0.0508 and 0.127
	2353	93.88	0.056	400.43		
	1566	62.48	0.084	393.78		
	2353	93.88	0.084	591.67		

Table 2 SLE values at selected locations for every test and the largest R_a value and cutting time

Test		SLE values (μm) at location, x (mm)						Largest R_a value (μm)	Cutting time (min)
		12.75	38.1	76.2	114.3	150.0	Max SLE (at X)		
Ramp	1	−8.72	−0.93	0.054	8.56	−13.06	19.28 (108.07)	1.68	12.18
	2	10.82	15.02	1.32	9.97	11.79	15.05 (38.21)	1.06	8.02
	3	22.49	14.40	−29.11	9.72	33.27	33.27 (150.00)	2.09	8.13
	4	37.65	9.01	−52.73	4.34	35.08	−54.60 (75.99)	1.72	5.41
Contour	1	−7.18	−4.41	−7.29	11.98	−8.31	18.63 (109.75)	1.69	12.87
	2	−16.37	−3.37	5.41	12.38	−19.37	−19.37 (150.00)	1.58	7.72
	3	5.63	−2.88	−17.40	6.42	36.25	36.25 (150.00)	2.04	7.91
	4	18.57	−2.84	−32.57	6.07	16.06	−41.89 (76.95)	1.33	5.33
Peripheral	1	37.91	−0.28	−41.92	−1.52	60.99	60.99 (149.40)	0.343	0.633
	2	72.86	12.84	−13.96	−1.96	90.07	90.07 (150.00)	0.363	0.415
	3	90.30	16.03	−92.05	−2.40	94.38	94.38 (150.00)	0.331	0.423
	4	51.95	2.78	−51.03	−3.23	69.00	69.00 (149.87)	0.507	0.279
	5	19.45	2.04	−13.16	−3.40	24.12	24.12 (150.00)	0.641	0.633
	6	114.38	22.88	−120.22	−5.45	127.85	−130.05 (77.02)	0.488	0.415
	7	66.52	11.77	−67.91	−3.85	75.99	76.73 (149.12)	0.467	0.423
	8	62.61	10.15	−53.77	−4.96	69.99	74.10 (148.81)	0.993	0.279

locations where undercut or overcut is observed to be prominent (see Fig. 4 and Table 2). The maximum SLE value for this amount of feed rate increase is also tremendously high (1.75 to 3.5 times). This reveals that the skidding of the ball nose end mill at a higher feed rate tends to be significantly high with a nonlinear relationship. It is also observed in Fig. 6 that an increase in feed rate obviously influences the cutting forces due to larger chip load. However, with the similar amount of cutting speed increase from 62.48 to 93.88 m/min (i.e., 1.5 times), the SLE values at different locations are found to be seldom influenced. In fact, a higher cutting speed, for example, 93.88 m/min at a fixed feed rate of 0.056 mm/tooth was found to perform better in term of SLE values at all five prominent locations and the maximum SLE for the whole machined surface. This states that a higher cutting speed tends to result in a better dimensional accuracy, may be due to the fact that the tool has a higher momentum to smoothen the machined surface. Lower surface roughness values observed at higher cutting speeds for any given feed rate support this hypothetical statement. Therefore, by observing the SLE and roughness values listed in Table 2 and overall SLE profiles presented in Fig. 4 for ramp milling, it can be concluded that the cutting conditions in test no. 2 (0.056 mm/T and 93.88 m/min) provided the most promising performance. Moreover, this condition requires less machining time due to comparatively a higher cutting speed as compared to test no. 1.

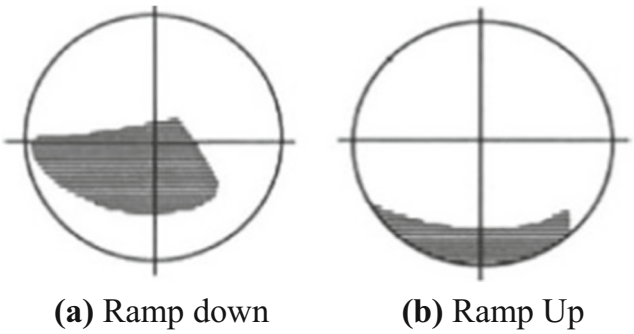

Fig. 5 Chip area when ramp milling a curved surface vertically with ball nose end mill [27]

3.2 Contour milling

During contour milling, the feed direction had to change in each region in order to maintain conventional (down) milling. When down stepping on concave and convex surfaces (regions I and IV, respectively), the tool feed was directed in the negative Y-direction, and it was in the positive Y-direction when up stepping for regions II and III. SLE values at five selected locations for the four different cutting conditions in contour milling are presented Table 2. Also, Fig. 8 depicts the plots of the SLE values along the surface for the four contour milling tests, and the magnitude of the associated force data is plotted in Fig. 9. The SLE plots in this case tend to be almost similar as compared to ramp milling. Again, this expectation can be explained partially by understanding chip load. The chip removed at the same inclination angle is approximately the same for stepping down the curve and stepping up the curve for both concave and convex surfaces. As inclination angle increases, the chip area removed decreases which results in lower force and less tool deflection. This is verified in the force plots. The two peaks are due to the ploughing action as explained in Sect. 3.1 for the case of ramp milling.

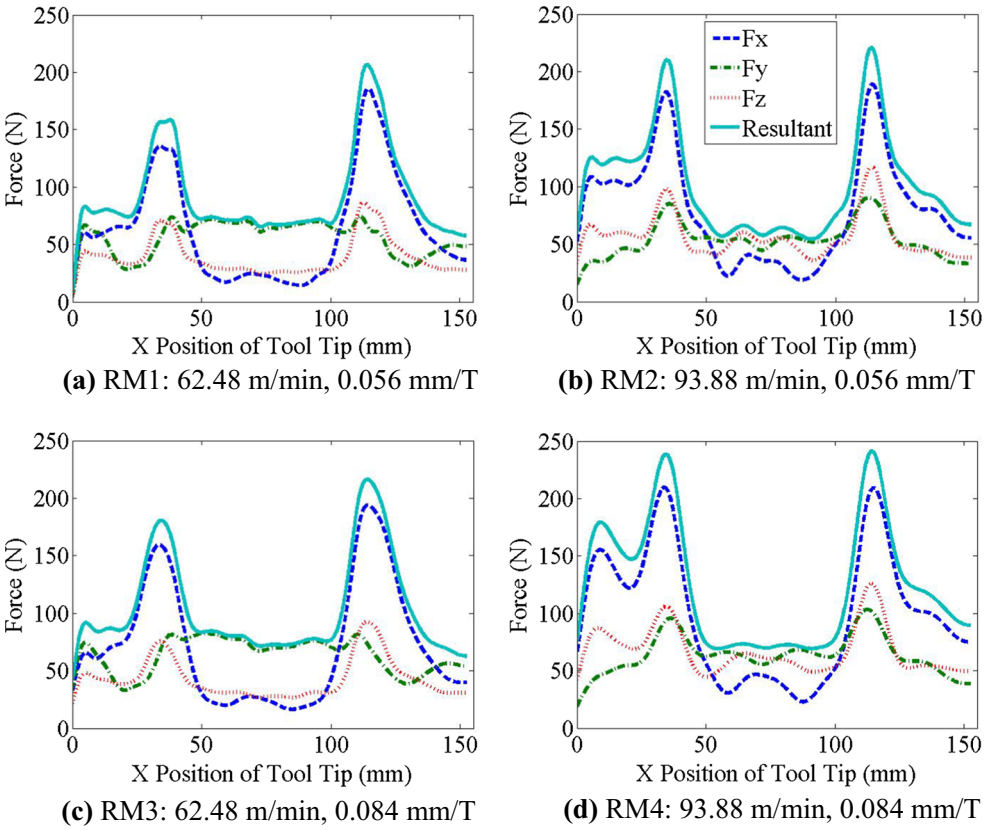

Fig. 6 Cutting force components and their resultant values against plate length in x-direction for four different conditions in ramp milling of the S-curve

When comparing the machining performance, the effect of cutting conditions is also found to be in similar trend as observed for ramp milling (see Table 2). Higher feed rates at any given cutting speed resulted in larger SLE values, and again, that may be due to higher skidding effect. While comparing the cutting speeds at the lowest feed rate of 0.056 mm/tooth, a higher cutting speed did hardly affect both the SLE and roughness values. As cutting time needed for contour milling test no. 2 (0.056 mm/tooth, 93.88 m/min) is significantly lower as compared to the test no. 1 (0.056 mm/tooth, 62.48 m/min) and difference of both SLE and roughness values for both test nos. 1 and 2 is insignificant, it can be concluded that the cutting condition in test no. 2 is the best among all four conditions tested.

3.3 Peripheral milling

SLE values in peripheral milling obtained at five selected locations for the eight different cutting conditions are presented in Table 2. While four cutting conditions are same as ramp or contour milling by combining cutting speed and feed rate, two different radial depths of cut are considered for faster machining and, thus, productivity. However, the radial DOC in peripheral milling is still kept lower than the other two

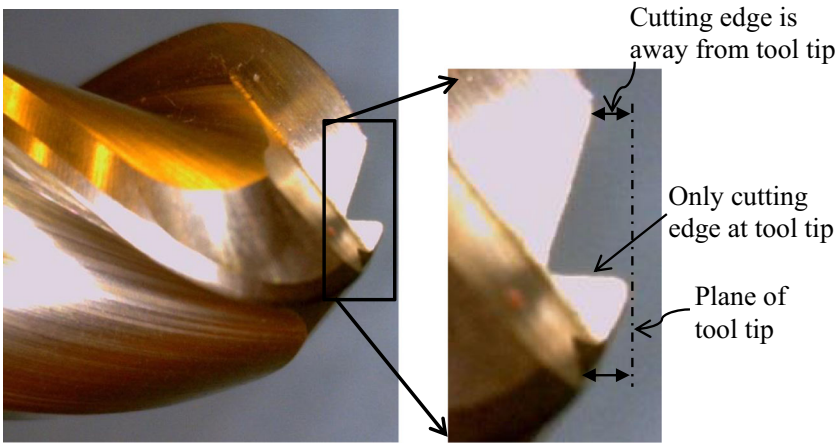

Fig. 7 Geometry of cutting edges and tool tip of a three-flute ball nose end mill

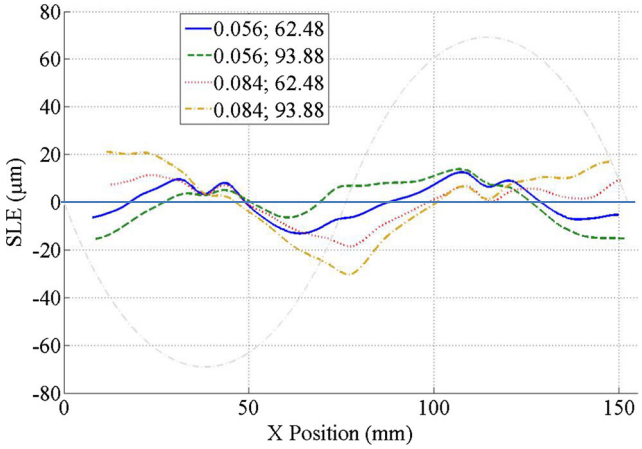

Fig. 8 Surface location error for contour milling path

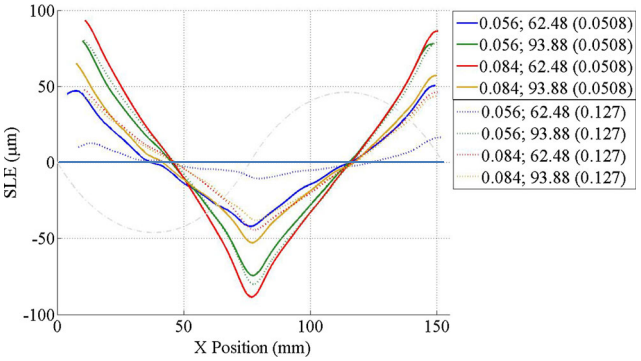

Fig. 10 Surface location error for peripheral milling path

techniques in order to avoid its cantilever deflection as the tool engages with the workpiece across the entire plate thickness and thus experiences comparatively higher cutting loads. Note that, in case of ramp and contour milling techniques, axial DOCs can be considered in a limited range due to the ball shape geometry of the tool. Figure 10 shows the SLE along the surface for the eight peripheral milling tests. The force data for the tests at radial DOCs of 0.0508 and 0.127 mm are displayed in Figs. 11 and 12, respectively.

The SLE plots for peripheral milling tend to be similar to ramp and contour milling presented in Sects. 3.1 and 3.2, respectively. The cutting mechanics in peripheral milling may be different because the tool periphery with constant diameter engages with the workpiece, and thus, skidding of tool in this case is invalid. However, the feed direction (x-axis) is the cause in peripheral milling. When machining regions I and IV, the tool is traveling away from the workpiece before it completely feeds into the workpiece, which in turn causes undercut error. In contrast, when milling in regions II and III, the tool is moving into the workpiece in each rotation. This causes more material removal as well as material suppression, which results in overcut or negative SLE value.

As seen in Table 2, a higher feed rate (mm/tooth) at a given cutting speed negatively affects the SLE value. It is due to a comparatively larger chip load and the cantilever action of the tool for over the entire plate thickness while cutting material at a higher feed rate. Force data in Figs. 11 and 12 support this

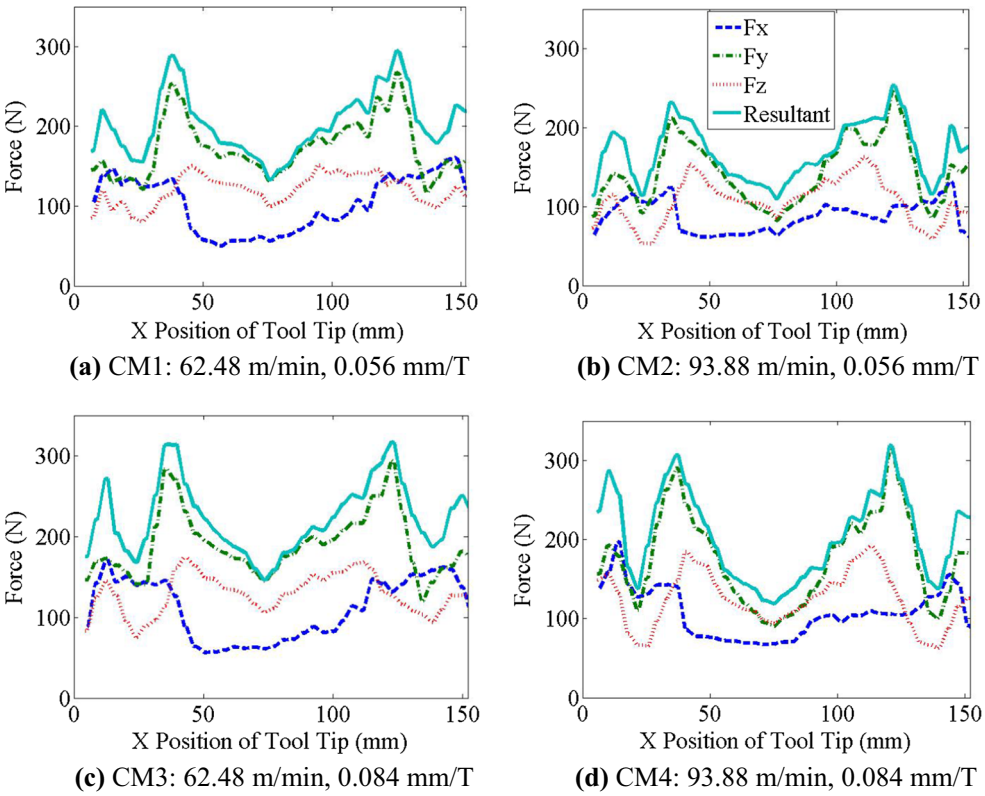

(a) CM1: 62.48 m/min, 0.056 mm/T

(b) CM2: 93.88 m/min, 0.056 mm/T

(c) CM3: 62.48 m/min, 0.084 mm/T

(d) CM4: 93.88 m/min, 0.084 mm/T

Fig. 9 Cutting force components and their resultant values against plate length in x-direction for four different conditions in contour milling of the S-curve

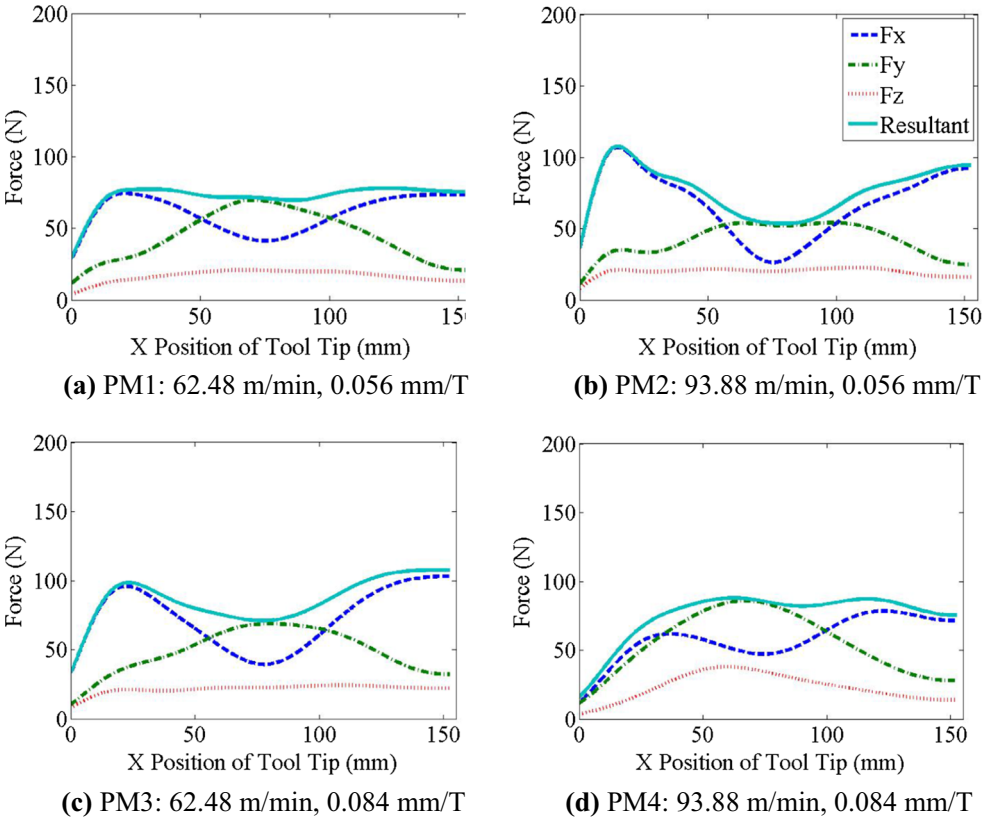

Fig. 11 Cutting force components and their resultant values against plate length in x-direction for four different conditions at radial depth of cut of 0.0508 mm in peripheral milling

(a) PM1: 62.48 m/min, 0.056 mm/T **(b)** PM2: 93.88 m/min, 0.056 mm/T

(c) PM3: 62.48 m/min, 0.084 mm/T **(d)** PM4: 93.88 m/min, 0.084 mm/T

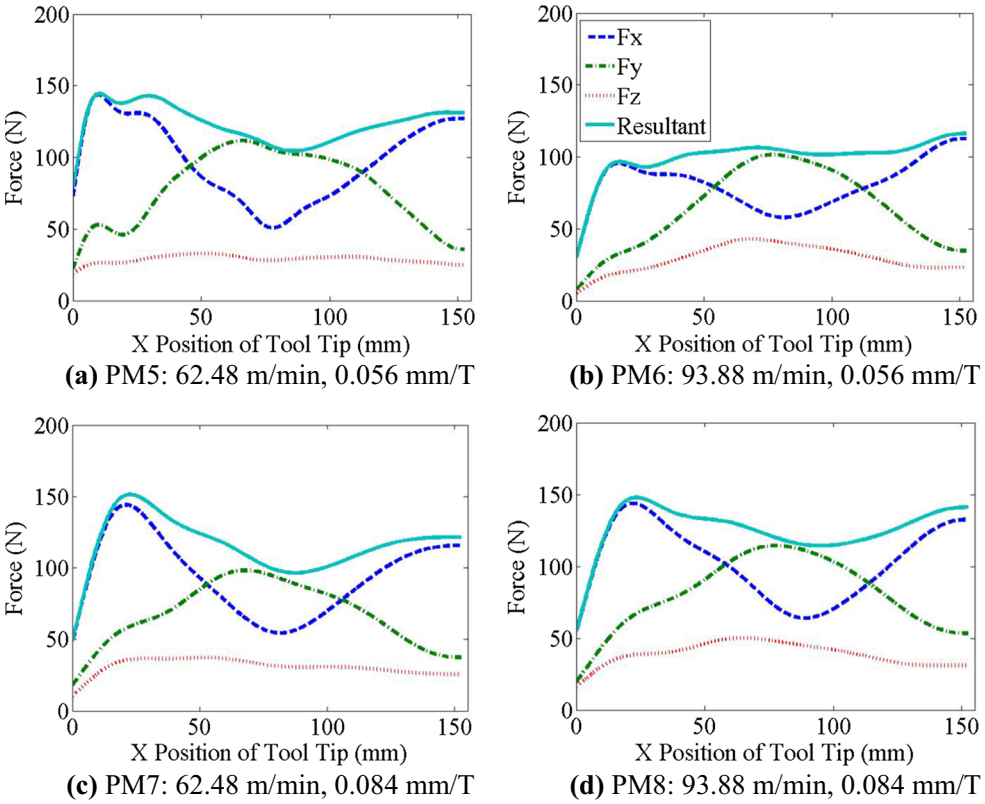

Fig. 12 Cutting force components and their resultant values against plate length in x-direction for four different conditions at radial depth of cut of 0.127 mm in peripheral milling

(a) PM5: 62.48 m/min, 0.056 mm/T **(b)** PM6: 93.88 m/min, 0.056 mm/T

(c) PM7: 62.48 m/min, 0.084 mm/T **(d)** PM8: 93.88 m/min, 0.084 mm/T

statement. However, it is also interesting to observe that higher radial DOCs offer overall less SLE values at all five locations (see Table 2 and Fig. 10). It may be due to higher stability of tool with better gripping with the workpiece while cutting progresses. It can be noted that increasing in radial DOC does not reduce machining time. Table 2 also shows that the roughness values increase with the increase in radial DOC. It is due to the radial geometry of the tool that feeds into the workpiece in each rotation, while other conditions are kept fixed. As the SLE value is the primary consideration for machining performance, repeated tests confirm that the cutting condition test no. 5 (0.056 mm/tooth, 62.48 m/min, 0.127-mm radial DOC) is optimum among all eight tests for peripheral milling.

It is also noticed that the peripheral milling technique offers much improved surface roughness as compared to both the ramp and contour milling. It is due to the fact of the tool geometry while engaging with the workpiece during cutting. In case of peripheral cutting, the whole plate or curved wall surface is machined with a single pass of the tool and it engages with the workpiece like a straight contact line across the plate thickness. So, the resulting surface becomes very smooth, though it is influenced by radial DOC in each rotation of the tool. However, in the cases of ramp and contour milling, the surface was machined with several passes of the tool as the tool cannot engage across the plate thickness with its limited ball shape geometry near the tip. As several passes are needed, the ball shape geometry forms grooves between the tool passes, and this in turn affects surface finish.

3.4 Comparison between the milling tool path strategies

Surface location error (SLE) and average surface roughness values during ramp, contour, and peripheral milling for S-curved surfaces are investigated and discussed in Sects. 3.1, 3.2, and 3.3, respectively. These machining performances, the machining time, and the best cutting conditions can be summarized as follows:

1. Ramp milling: maximum SLE 15.05 μm, average roughness 1.06 μm, and machining time 8.02 min at 0.056 mm/tooth feed rate, 93.88 m/min cutting speed with fixed 0.508-mm axial DOC, and 0.254 radial DOC (test no. 2),
2. Contour milling: maximum SLE 19.37 μm (−), average roughness 1.58 μm, and machining time 7.72 min at 0.056 mm/tooth feed rate, 93.88 m/min cutting speed with fixed 0.508-mm axial DOC, and 0.254 radial DOC (test no. 2)
3. Peripheral milling: maximum SLE 24.12 μm, average roughness 0.641 μm, and machining time 0.633 min at 0.056 mm/tooth feed rate, 62.48 m/min cutting speed, and 0.127-mm radial DOC (test no. 5).

The best SLE plot obtained for each milling path is again composed in Fig. 13 for comparison between milling strategies. While achieving minimum dimensional tolerance is the major challenge during machining of curved wall surfaces, the plots suggest that the ramp milling is the best among all techniques. It also outperforms the contour milling in terms of other machining performances including average surface roughness and machining time for the same amount of material removal. However, in terms of these later two machining performances, the peripheral milling technique is found to be very promising. As the tool requires one pass to machine the entire wall surface, the machining time drops significantly. For the 0.254-mm depth to be removed from the original surface, the peripheral milling requires 1.26 min (2×0.633 min) by passing the tool twice for at 0.127-mm radial DOC, while the ramp milling requires 8.02 min which is significantly high. Thus, there is a trade-off between the ramp and peripheral milling techniques. In summary, for the best SLE to be achieved, the ramp milling is preferable, whereas the peripheral milling is to achieve the best surface roughness and machining productivity.

4 Conclusions

On a vertical three-axis milling machine, experiments were performed machining parameters to investigate the least surface location error (SLE) and roughness values with minimum machining time during machining of stainless steel AISI 304. Ramp, contour, and peripheral tool path strategies at different machining conditions were studied for a 12.70-mm-thick S-curved wall surface that has both concave and convex geometry patterns and that resembles a mating surface commonly existing in different engine parts (e.g., turbine blades). Based on the study, the following conclusions can be drawn:

1. Both undercut (+SLE) and overcut (−SLE) of the surface are observed during milling with all milling strategies.

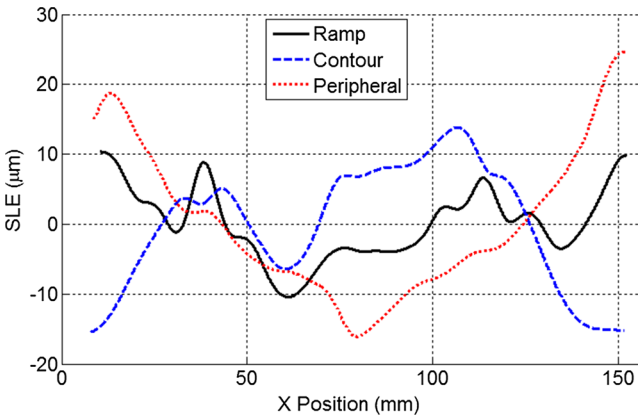

Fig. 13 SLE from the best cutting parameters for each milling path

Positive SLE is usually prominent during the downward feeding of the tool on both the concave and convex surfaces, while overcut is observed during upward tool feed. Such result is not obvious when milling flat 2D surface. Tool-workpiece respective inclination angle is a major factor in the amount of error produced.

2. Skidding of the tool on inclined surface is the reason why undercut happens during ramp and contour milling. In the case of peripheral milling, continuous tool movement away from the wall surface may be the reason for undercut error. However, overcut mainly happens due to the push by the tool that suppresses material within the desired surface level.
3. A lower feed rate and higher cutting speed offer better SLE and surface roughness values in case of ramp and contour milling. However, a higher cutting speed cannot be applied during machining with the peripheral milling because the tool engages the workpiece across the entire plate thickness, which causes higher chip load and cutting force leading to poor machining performance.
4. SLE values are found to be the lowest with ramp (15.05 μm), followed by contour (18.63 μm), and the highest with peripheral (24.12 μm) milling paths for the cutting conditions applied. However, peripheral milling may be preferable in terms of surface roughness (improved about 40 %) and overall machining time (six times faster than ramp milling). Therefore, there is a trade-off between the ramp and the peripheral milling with respect to the requirement of part quality and productivity.
5. Future work will investigate the effect of tool diameter and tool length extending from the tool holder. Also, the utilization of a fourth axis will enable the inclination angle to remain constant when milling in ramp and contour. This will lead to constant force on the tool and theoretically a more consistent SLE. A comprehensive model that correlates the experimental findings and skidding phenomenon should also be considered.

References

1. Ackerman RI, Albrecht RW Jr, Keith SR, Mcrae EE Jr (2002) Dovetail blade rotor and rotor grove configuration, European Patent, Publication number EP1288440 A2
2. Bounazef M, Guessasma S, Bedia EAA (2007) Blade protection and efficiency preservation of a turbine by a sacrificial material coating. Adv Powder Technol 18(2):123–133
3. Abou-El-Hossein KA, Yahya Z (2005) High speed end milling of AISI 304 stainless steel using new geometrically developed carbide inserts. In: Proc. 13th Int. Scientific Conference on Achievements in Mechanical and Materials Engineering. Gliwice, Poland
4. Kita Y, Furuike H, Nakagawa H, Hirogaki T (2001) Basic study of ball end milling on hardened steel. J Mater Process Technol 111(1–3):240–243
5. Ikua BW, Tanaka H, Obata F, Sakamoto S (2001) Prediction of cutting forces and machining error in ball end milling of curved surfaces—I theoretical analysis. Precis Eng 25(4):266–273
6. Ikua BW, Tanaka H, Obata F, Sakamoto S, Kishi T, Ishii T (2002) Prediction of cutting forces and machining error in ball end milling of curved surfaces—II experimental verification. Precis Eng 26(1): 69–82
7. Lim EM, Menq CH (1995) The prediction of dimensional error for sculptured surface productions using the ball-end milling process. Part 2: surface generation model and experimental verification. Int J Mach Tools Manuf 35(8):1171–1185
8. Baptista R, Simoes JA (2000) Three and five axes milling of sculptured surfaces. J Mater Process Technol 103(3):398–403
9. Yun WS, Cho DW (2000) An improved method for the determination of 3D cutting force coefficients and runout parameters in end milling. Int J Adv Manuf Technol 16(12):851–858
10. Lazoglu I (2003) Sculpture surface machining: a generalized model of ball-end milling force system. Int J Mach Tools Manuf 43(5): 453–462
11. Zhu R, Kapoor SG, DeVor RE (2001) Mechanistic modeling of the ball end milling process for multi-axis machining of free-form surfaces. J Manuf Sci Eng 123(3):369–379
12. Altintaş Y, Lee P (1996) A general mechanics and dynamics model for helical end mills. CIRP Ann Manuf Technol 45(1):59–64
13. Bouzakis KD, Aichouh P, Efstathiou K (2003) Determination of the chip geometry, cutting force and roughness in free form surfaces finishing milling, with ball end tools. Int J Mach Tools Manuf 43(5):499–514
14. Sun G, Wright P (2005) Simulation-based cutting parameter selection for ball end milling. J Manuf Syst 24(4):352–365
15. Insperger T, Gradišek J, Kalveram M, Stepan G, Winert K, Govekar E (2006) Machine tool chatter and surface location error in milling processes. J Manuf Sci Eng 128(4):913–920
16. Subrahmanyam KVR, San WY, Soon HG, Sheng H (2010) Cutting force prediction for ball nose milling of inclined surface. Int J Adv Manuf Technol 48(1–4):23–32
17. Wojciechowski S, Twardowski P, Pelic M (2014) Cutting forces and vibrations during ball end milling of inclined surfaces. Procedia CIRP 14:113–118
18. Watanabe T, Iwai S (1983) A control system to improve the accuracy of finished surfaces in milling. J Dyn Syst Meas Control 105(3):192–199
19. Yang MY, Choi JG (1998) A tool deflection compensation system for end milling accuracy improvement. J Manuf Sci Eng 120(2): 222–229
20. Budak E, Altintas Y (1994) Peripheral milling conditions for improved dimensional accuracy. Int J Mach Tools Manuf 34(7):907–918
21. Altintas Y (1994) Direct adaptive control of end milling process. Int J Mach Tools Manuf 34(4):461–472
22. Rao VS, Rao PVM (2006) Tool deflection compensation in peripheral milling of curved geometries. Int J Mach Tools Manuf 46(15): 2036–2043
23. Rao VS, Rao PVM (2005) Modelling of tooth trajectory and process geometry in peripheral milling of curved surfaces. Int J Mach Tools Manuf 45(6):617–630
24. Rao VS, Rao PVM (2006) Effect of workpiece curvature on cutting forces and surface error in peripheral milling. Proc Inst Mech Eng B J Eng Manuf 220(9):1399–1407
25. Tlusty J, Zaton W, Ismail F (1983) Stability lobes in milling. CIRP Ann Manuf Technol 32(1):309–313
26. Li HZ, Zeng H, Chen XQ (2006) An experimental study of tool wear and cutting force variation in the end milling of Inconel 718 with coated carbide inserts. J Mater Process Technol 180(1):296–304
27. Toh CK (2004) A study of the effects of cutter path strategies and orientations in milling. J Mater Process Technol 152(3):346–356